

Koopman-driven grip force prediction through EMG sensing

Tomislav Bazina, Ervin Kamenar, Maria Fonoberova, Igor Mezić, *Fellow, IEEE*

Abstract—Loss of hand function due to conditions like stroke or multiple sclerosis significantly impacts daily activities. Robotic rehabilitation provides tools to restore hand function, while novel methods based on surface electromyography (sEMG) enable the adaptation of the device's force output according to the user's condition, thereby improving rehabilitation outcomes. This study aims to achieve accurate force estimations during medium wrap grasps using a single sEMG sensor pair, thereby addressing the challenge of escalating sensor requirements for precise predictions. We conducted sEMG measurements on 13 subjects at two forearm positions, validating results with a hand dynamometer. We established flexible signal-processing steps, yielding high peak cross-correlations between the processed sEMG signal (representing meaningful muscle activity) and grip force. Influential parameters were subsequently identified through sensitivity analysis. Leveraging a novel data-driven Koopman operator theory-based approach and problem-specific data lifting techniques, we devised a methodology for the estimation and short-term prediction of grip force from processed sEMG signals. A weighted mean absolute percentage error (wMAPE) of $\sim 5.5\%$ was achieved for the estimated grip force, whereas predictions with a 0.5-second prediction horizon resulted in a wMAPE of $\sim 17.9\%$. The methodology proved robust regarding precise electrode positioning, as the effect of sensing position on error metrics was non-significant. The algorithm executes exceptionally fast, processing, estimating, and predicting a 0.5-second sEMG signal batch in just ~ 30 ms, facilitating real-time implementation.

Index Terms—Koopman operator theory, electromyography, grip force estimation, robotic rehabilitation

I. INTRODUCTION

THE concept of sensing gripping force from muscle activity through the non-invasive surface electromyography (sEMG) method is based on a group of muscle fibers called motor units (MU), which are activated by brain motor neurons.

This work was supported by the U.S. Air Force Office of Scientific Research (AFOSR) under Award FA9550-22-1-0531 and by the University of Rijeka under Grant uniri-iskusni-tehnic-23-47. (Corresponding author: Ervin Kamenar).

Tomislav Bazina is with the University of Rijeka, Faculty of Engineering, 51000 Rijeka, Vukovarska 58, Croatia (e-mail: tomislav.bazina@uniri.hr).

Igor Mezić is with the University of California, Santa Barbara, CA, 93101 USA (e-mail: mezc@ucsb.edu).

Ervin Kamenar is with the University of Rijeka, Faculty of Engineering, 51000 Rijeka, Vukovarska 58, Croatia (e-mail: ekamenar@uniri.hr).

The authors are with AIMdyn, Inc., Santa Barbara, CA, 93101, USA (e-mail: tomislav@aimdyn.com; mezc@aimdyn.com; mfonoberova@aimdyn.com; ervin@aimdyn.com).

The EMG signal is obtained as an interference of firing signals from each MU, known as motor unit activation potential (MUAP). Factors such as electrode placement, size, and inter-electrode distance, as well as tissue characteristics (such as fat layers and skin conductivity), temporal and spectral characteristics of the firing patterns, and cross-talk from neighboring muscles, all influence the variability of the EMG signal [1].

In [2], the authors predicted pinching force using a 6-channel sEMG sleeve, focusing on the RMS feature of the signal. They employed the gene expression programming algorithm and reported RMSE errors of 7.5–8.5% and cross-correlation coefficients up to 95%. The study examined four MVC levels (20%, 40%, 60%, and 80%) but did not test predictions near the transient states between these levels. In [3], the authors used sEMG with four bipolar electrodes on the forearm and finger force signals to predict grip force. They employed five EMG features and eleven finger force features, achieving a mean accuracy of 90% for grip force prediction in the transient phase. The study found that optimal sensing stabilized at three positions with 2–4 features. Electrode positioning on the forearm for grip force sensing was also explored in [4]. The study identified the brachioradialis muscle as optimal based on EMG signal strength. In [5], EMG signals were acquired using an eight-channel Myo's armband, and an LSTM network predicted normalized pinching force 1, 3, and 5 seconds ahead directly from the EMG data. Based on [6], which used eight sEMG sensors and 24 healthy subjects, extrinsic muscle coordination reliably predicted grip and pinch force levels due to its greater sensitivity to force changes compared to intrinsic muscles. Some studies, including [7] and [8], have focused on predicting gripping force from the transient phase of EMG signal, which is the initial burst when the muscle begins exerting force. In [7], a high-density 192-channel sEMG sensor setup was employed on 12 subjects to predict grasp force. This prediction utilized ten features and regularized linear regression, achieving absolute errors as low as 2.5% of MVC. Additionally, in [8], online predictions of gripping force were obtained from 8 sEMG sensors placed on the forearms of 16 participants. The model included ten features extracted from the EMG signal. Predictions were made 330 ms ahead using the elastic net regression algorithm, resulting in errors of 2% of MVC.

It is evident from the above analysis, as well as the findings highlighted in [9], that while the majority of the research has achieved favorable results in terms of accuracy, it relies on a high—and constantly increasing—number of necessary

sEMG sensors for the accurate prediction of grasping force. Additionally, existing methods often overlook advanced signal processing techniques, which are crucial for extracting the meaningful portion of the raw EMG signal. This signal is essential for causal modeling of grip force but is consistently affected by noise. Moreover, forecasts during the transient state are rarely taken into account. Our research is the first to develop an online modeling and signal-processing framework for estimating and short-term forecasting grip force based on Koopman operator theory (KOT) [10]. The main contributions of this work are as follows:

- We devised and optimized a composition of EMG signal processing methods, achieving high peak cross-correlations between EMG and grip force signals using a single sensing position on the forearm.
- We devised a novel Koopman-based data-driven approach with problem-specific observables for estimating and short-term predicting grip force in real-time during both transient and plateau phases.
- The devised methodology enables fast execution, thus facilitating real-time implementation.

II. MATERIALS AND METHODS

This study involves obtaining time-series data on human muscle activity through sEMG and measuring hand grip force with a manual dynamometer. The dynamometer's shape necessitated a medium wrap type of grasp, following the taxonomy developed by [11] and further refined by [12]. This approach contrasts with some studies, such as [4], which use the strength of the EMG signal as a criterion for predicting grip force.

To minimize prediction errors, we considered sEMG positioning on the forearm to maximize signal measurement. Advanced signal processing techniques were employed to extract relevant features from the EMG signals and establish a robust correlation with grip force. Offline optimization of decision variables was also conducted.

A crucial aspect of the research involves the signal filtering step, essential for proper inferences using EMG signals, which are often largely affected by noise and cross-talk between muscles. The signals are typically processed using notch filtering at 50 Hz to eliminate ground noise [3], bandpass filtering between approximately 10 and 500 Hz to remove wire movement artifacts [6]–[9], bandpass filtering between 100 and 500 Hz [4], and bandpass filtering that captures only power spectrum peaks between 20 and 60 Hz [5]. In contrast to such "general" filtering approaches, we focused on signal processing aimed at extracting only meaningful features (comparable to observables in KOT) from the sEMG signal—those highly correlated with grip force—that can later be applied within the KOT framework for accurate modeling and prediction. This strategy reflects elements of the structural approach to sEMG modeling in [1], which states that recruiting MUs is fundamental for generating muscle force. When more MUs are recruited, the muscle produces greater force, and the firing rate of each MU further amplifies this force. Generally, MU firing rates increase almost linearly with the muscle's force output. These firing patterns and the interference between the active

MUs influence the characteristics of the measured sEMG. We aim to isolate the difficult-to-identify signal components, specifically the recruited MUs, their interference patterns, and firing rates that predominantly contribute to measured grip force during a medium wrap. This approach helps separate the meaningful signal from unwanted noise. We utilized Fast Fourier Transformation (FFT) and sensitivity analysis (SA) to develop a spectral mask that selectively targets specific spectral components to achieve this. The aim is to develop a fully integrated module for EMG signal preprocessing, including calibration and normalization. Additionally, the module will incorporate grip force prediction using the KOT.

In Section II-A, we describe the hardware components and their calibration. Section II-B explains the composition of EMG signal processing steps and describes the SA and optimization methods. Finally, Section II-C delves into the details of the Koopman methodology used for predicting and estimating hand grip force from EMG signals.

A. Experimental Setup & Design

Two different sensing devices were used during the experimental phase: Shimmer3 EMG Unit¹ for muscle activity sensing and Vernier Go Direct® Hand Dynamometer² for grip force measuring. Both devices are wireless and connect to PC through Bluetooth. The EMG sensing unit records the electrical activity on the skin surface associated with muscle contractions. It can capture response signals from entire muscle groups but is commonly prone to noise. In the performed experiments, the EMG sampling rate was set to 1 kHz. A maximum internal gain of 12 was used, and an internal calibration procedure was followed. The dynamometer, with a force range of 0 to 550 N, a resolution of 0.05 N, and an uncertainty of 1.96 standard deviations (95% confidence interval), was used at a sample rate of 200 Hz.

Before performing experiments, the reference dynamometer was calibrated in-house according to ASTM E74: *Standard Practices for Calibration and Verification for Force-Measuring Instruments* norm. Calibration weights of OIML classes F1, M1, and M3 were used, and the laboratory temperature was maintained at approximately 23°C. Calibration forces ranged from 0 to 550 N in steps of 5, 20, 50, 100, 150, 200, 250, 300, 350, 400, 450, 500, and 550 N. The instrument was first preloaded from minimum to maximum force to establish hysteresis. Each measurement was preceded by reducing the instrument to zero between successive loadings, and the entire process was repeated three times. For measured forces greater than 50 N, the uncertainty as a percentage of the measured force is less than 4%, while for forces below 50 N, the percentage can be as high as 10%. The obtained calibration equation that relates the raw dynamometer signal g_r to the reported grip force g is:

$$\hat{g} = 1.0629g_r - 2.5880 \times 10^{-4}g_r^2 - 9.0028 \times 10^{-8}g_r^3 + 7.6152 \times 10^{-10}g_r^4. \quad (1)$$

¹<https://shimmersensing.com/product/shimmer3-emg-unit/>

²<https://www.vernier.com/product/go-direct-hand-dynamometer/>



Fig. 1: Placement of sEMG electrodes near flexor carpi ulnaris muscle on the forearm: (a) Position 1 (P1) and (b) Position 2 (P2).

Although the most prominent term in (1) is linear and close to 1, a fourth-degree polynomial was deemed necessary due to the strict demands of the ASTM E74 norm.

The Robot Operating System (ROS) and Python were utilized to integrate devices and enable the acquisition of time-series raw EMG and calibrated dynamometer signals across all experiments. The implemented modules are available in the first author's GitHub repositories, namely `godirect_ros`³ and `shimmer_ros`⁴.

We aim to accurately predict grip force using two electrodes positioned at one sensing location, with a third (neutral) electrode serving as a reference in the final setup. This configuration is used because the EMG signal is typically very small relative to environmental noise, such as interference from power sources. Common Mode Rejection (CMR) takes advantage of the fact that environmental noise affects all electrodes similarly. By subtracting one signal from another, the common noise is cancelled out, while the local EMG signal, which varies with electrode position, is preserved and amplified. This approach improves the clarity of the EMG signal despite significant background noise.

During the experimental design phase, a 2-factor randomized block design (RBD) [13] was selected as the appropriate design. In the preliminary phase, various positions for attaching electrodes were tested. Ultimately, two sensing positions on the human forearm, near the flexor carpi ulnaris muscle (see Fig. 1), were chosen for further analyses based on a simple screening experiment considering only signal strength. The electrode positioning corresponds to one of the configurations evaluated in previous studies [4], [9]. A subject variable is viewed as a nuisance during the design procedure. An experiment was conducted with 13 male volunteers aged 22 to 24⁵. Blocking was used to remove the effect of the subject, considered nuisance variable, allowing the effect of the measuring positions on estimation and prediction errors to be examined. Randomization was applied within each block. Prior to experiments, skin for each subject was prepared by removing hair near measured positions, while alcohol swabs were used to clean the skin at the measuring location. Each subject was allowed several minutes to prepare for the

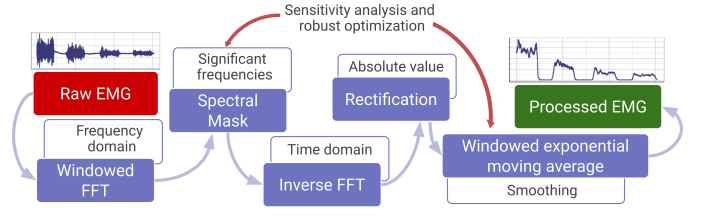


Fig. 2: Signal processing steps for obtaining optimal processed EMG regarding cross-correlation with measured grip strength.

experiment and adjust the grip to approximate the required five force levels. In all the experiments, the first 5 seconds of the acquired data were used to zero the dynamometer signal at the measuring position. The transitions between grip force levels were also recorded. Table I details the experimental design.

Subject Levels	Position levels	Grip force levels [%]	Repetitions	Runs
ac, dp, ds, js, lb, lk, lm, ln, md, mm, nk, pb, ss	1, 2	100, 75, 50, 25, 0	2	52

TABLE I: Summary of 2-factor RBD experiment.

B. Multi-step sensitivity analysis and procedural parameter optimization

The optimization procedure aims to maximize the peak cross-correlation between the processed EMG signal and the synchronously collected grip force. We performed multi-step SA to identify the most influential spectral components and narrow the optimal bounds for decision variables. Narrowing was achieved by examining scatterplot projections of individual decision variables with smoothed trends and means using Latin hypercube (LH) sampling. Simultaneous optimization and SA ensure that cross-correlations remain near their optimal values, even when small variations are introduced. This approach enhances local robustness, helping to avoid unstable maxima and maintain consistent performance.

First, data is processed in batches of approximately 0.5 seconds (496 data points) with a sampling rate of 992.97 Hz for EMG signals. Each batch is transformed into the frequency domain using FFT, achieving a resolution of 2.002 Hz. A spectral mask, obtained through an optimization process, is then applied to attenuate or amplify frequency components selectively. After modifying the amplitudes, an inverse FFT reverts the signal to the time domain. Signal rectification is performed by taking the absolute value, followed by windowed exponential moving average (MA) smoothing. The smoothing window is applied within each batch, except for the first (window size - 1) points, where data from the previous batch is utilized. In addition to the spectral mask, the optimization also targets finding the optimal window size and decay factor for exponential smoothing. The entire process for obtaining optimal processed EMG signal is schematically outlined in Fig. 2. The high-dimensional optimization problem was formulated to maximize the mean peak cross-correlation across all measurements using a decision vector comprised of 250

³https://github.com/tbazina/godirect_ros

⁴https://github.com/tbazina/shimmer_ros

⁵Informed consent was obtained from all human subjects involved.

variables. The entries and initial bounds of the decision vector are:

- Spectral mask with 248 entries corresponding to each frequency bin (without DC offset) ranging from 0–5,
- Exponential smoothing window size ranging from 2–495,
- Exponential smoothing decay factor ranging from 0–0.05.

The DC offset was set to zero and excluded from the optimization process. Initial mask bounds were set within the 0–5 range, allowing either complete removal of a spectral component's amplitude or amplification by up to five times. In contrast, the decay factor bounds were designed to support simple MA (if set to 0) and exponential MA (if greater than 0). Broad bounds on the window size also enabled fine-tuning of the applied smoothing. The objective function for optimization was defined as the peak cross-correlation between the processed EMG signal and measured grip force. Since the problem is framed as a minimization, the function returns 1 minus the mean peak cross-correlation—yielding near-zero values for high cross-correlations and values close to one for low cross-correlations. Due to differences in sampling rates—where the EMG signal is sampled five times faster than the dynamometer—the grip force signal was resampled using EMG timestamps. Intermediate points were estimated using linear regression to ensure proper signal alignment for cross-correlation computation. We hypothesize that not all 248 FFT frequency bins significantly impact the cross-correlation. To address this, a multi-step SA is conducted prior to optimization to narrow the problem's scope and identify the most influential spectral components. Preliminary SA is performed first with grouped spectral mask variables to gain higher-level insight into cross-correlation sensitivity to smoothing and filtering. Grouped Sobol variance-based SA was performed separately on each dataset, corresponding to two EMG measurement positions (see Fig. 1). For each position, 65536 (2^{16}) samples of 250-dimensional decision vectors were generated using Saltelli's sampling scheme. Bootstrapping with 2^{16} resamples was applied to account for uncertainty, creating additional datasets by sampling the original one with replacement. Sensitivity indices (SI) were then calculated for each bootstrapped dataset, and empirical distributions were generated. From these distributions, 95% confidence intervals were derived. Fig. 3a presents the obtained first-order and total-order SI. The sum of all three first-order and total-order indices approximates 1, indicating that they can reliably approximate the percentage of output variance attributable to each variable, and interactions between variables can be safely ignored. When sampling the problem within the initial bounds, the contributions of smoothing parameters and the spectral mask to the variance in mean peak cross-correlation depend on the measurement position. Smoothing window size is the most influential factor, explaining between 47% and 65% of the output variance in peak cross-correlation for both positions. The decay factor contributes approximately 20–24%, while the frequency mask shows the most variance, ranging from 14% on P1 to 37% on P2. Additional LH sampling with 10,000 decision vector samples was conducted within the same bounds to investigate the partial contributions of smoothing parameters further. Fig.

3b displays the resulting projections onto the decay factor and window size. Increasing the window size improves the peak cross-correlation until it reaches a plateau, supporting the decision to narrow the window size bounds to the 200–495 range for subsequent SA steps. Conversely, increasing the decay factor shows a decreasing trend in peak cross-correlation, so we further narrowed the range to 0–0.01. The grouped SA was repeated with the narrowed parameter bounds, where the spectral mask contributed to 88% of the variance in P1 and 95% in P2. This highlights the necessity of ungrouping the mask for more detailed analysis in the subsequent steps.

The goal of iterative multi-step ungrouped SA is to reduce the dimensionality of the optimization problem by decreasing the number of spectral mask frequencies and identifying the ones that contribute most to the mean peak cross-correlation variance. This time, a more efficient RBD-FAST SA method [14] was used, returning only first-order SIs, with 65536 decision vector samples and resampling with bootstrapping using 8192 (2^{13}) samples for CI computation. After each step, the projections on the most sensitive spectral components, or smoothing parameters, were visualized using LH sampling with 10000 samples, and manual bounds narrowing was performed. The first step identified the 2 Hz spectral component as the most influential on cross-correlation variance, with an SI in the 78–83% range. The LH sample projection onto the 2 Hz component showed that increasing its mask variable significantly reduces the mean peak cross-correlation, prompting narrowing of its variable bounds to the 0–0.5 range. Additionally, LH sampling was projected onto the next three spectral components with the highest SI from the first SA step. Similar trends to those observed for the 2 Hz component were noted, prompting the narrowing of bounds to 0–1 for 4 Hz, 0–2 for 6 Hz, and 0–3 for 50 Hz. Another 18 steps (2–19) of iterative SE were performed similarly, and the top spectral components with narrowed bounds after each step are presented in Figure 4. Figures displaying LH sampling projections, along with smooth and mean lines that support the reasoning behind the narrowing of bounds, can be found in the first author's GitHub repository⁶. In a step-by-step analysis, a reverse funnel-shaped pattern can be observed (indicated by the two red arrows), with one starting point at low-frequency components and the other around 50 Hz. This pattern highlights the transition from the most influential spectral components to the less influential ones.

After the 19th step of ungrouped RBD-FAST SA (Fig. 4), the sum of all SIs corresponding to frequency masks ≥ 204 Hz amounted to less than 2% contribution. Therefore, the highest spectral component considered for further analysis was 202 Hz. This is consistent with [15], which indicates that most of the sEMG power spectrum is concentrated below 250 Hz. Next, LH sampling was performed twice within the newly obtained parameter ranges, followed by plotting and visually inspecting the influence trend of each of the 201 remaining spectral components (2–202 Hz). The mean and smooth lines were examined to narrow the bounds further

⁶<https://github.com/tbazina/grip-emg-optimize>

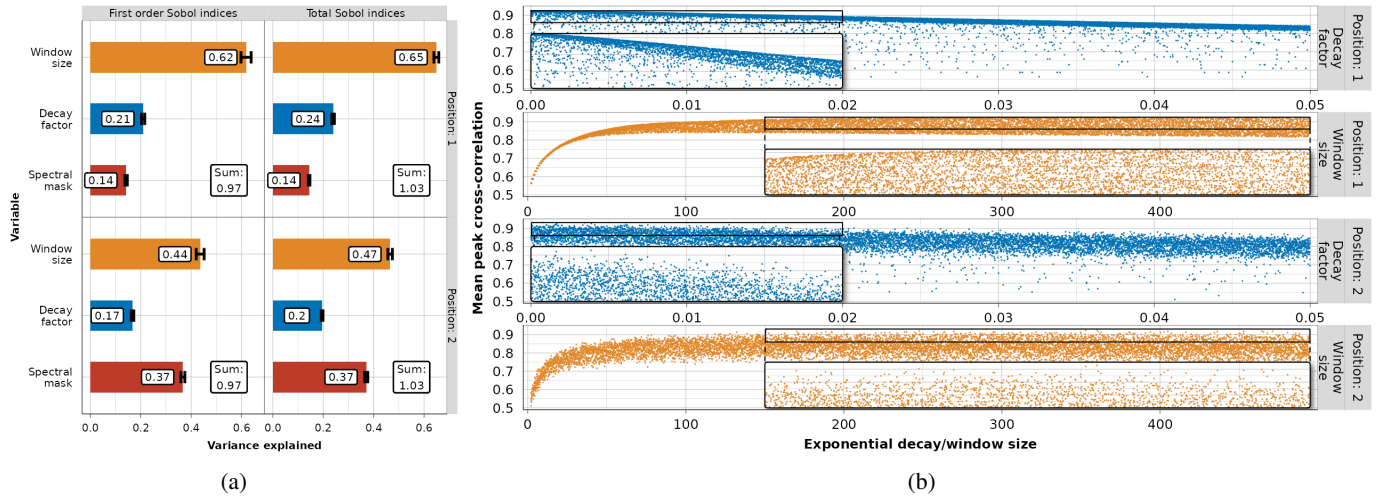


Fig. 3: Preliminary sensitivity analysis for two sensing positions: (a) first-order and total-order sensitivity indices, and (b) LH sampling projections onto the decay factor and window size variables.

around the optimal point visually. In the last two steps (20th and 21st), optimal bounds were identified (Fig 4) and used as the final cutoff values. Optimal smoothing parameters reveal interesting trends:

- Increasing decay factor decreases peak cross-correlation, and optimal values are close-to-zero ($0-5 \times 10^{-4}$), indicating a need for simple MA.
- Window size shows an optimum in the 275–330 range.

The description of the optimal spectral mask is detailed in Section III. With the optimal set of signal-processing procedures and parameters presented, the following section outlines the Koopman-driven methodology for estimating and predicting grip force from the processed EMG signals.

C. Koopman-driven estimation and prediction of hand grip force

The first part of this subsection briefly introduces the KOT and relevant literature, while the second and third detail its application to grip force estimation and prediction, respectively. The entire framework is designed so that the subject first performs a one-time, 20–30-second calibrating experiment simultaneously using sEMG sensors and a dynamometer, with grip force levels approximating those in Table I. Then, the meaningful processed EMG signal is obtained, and the estimation model is trained on the entire calibrating dataset. The estimation model is then used in batch processing to approximate grip force from the processed EMG, using only the data under the window. The obtained approximation is finally used to forecast grip force over a 0.5-second horizon or for the next batch.

The state-space representation of a dynamical system involves defining an n -dimensional state space manifold, denoted by M . The states \mathbf{x} belong to M , and the discrete-time evolution of the system is given by:

$$\mathbf{x}_{i+1} = \mathbf{F}(\mathbf{x}_i), \quad (2)$$

Here, \mathbf{F} is the potentially nonlinear state transition function $\mathbf{F} : M \rightarrow M$, and \mathbf{x}_{i+1} represents the time-shifted state.

Modeling a system in state space generally requires capturing nonlinearities, which are essential for accurately describing dynamical behavior but can be highly complex or even impossible. To address this challenge, we adopt an operator-theoretic perspective on the dynamics of observables [10]. The behavior of the nonlinear system (2) is thus mapped onto the dynamics of observables of \mathbf{x} defined as $\phi(\mathbf{x})$. Please note that, due to the nature of the system in question, this work focuses specifically on real-valued observables, $\phi : M \rightarrow \mathbb{R}$.

Collecting all possible observables constitutes a vector space that is generally infinite-dimensional. The Koopman operator, \mathcal{K} , that describes the evolution of observables over a discrete time interval Δt , is defined as [16]:

$$\phi(\mathbf{x}_{i+1}) = \mathcal{K}\phi(\mathbf{x}_i) = \phi[\mathbf{F}(\mathbf{x}_i)]. \quad (3)$$

Remarkably, even if the underlying state space system is nonlinear, \mathcal{K} remains linear [10]. This linearity holds regardless of the specifics of the dynamics of the observables.

In contrast to the dynamical systems, the Koopman operator can also describe "static" nonlinear maps between different spaces [17] $M \rightarrow N$, a property that we use in this work for estimating grip force from processed EMG signals. Through lifting and proper choice of observables, we can describe nonlinear maps using spaces of observables and a linear mapping operator $\mathcal{K} : \mathcal{O}_M \rightarrow \mathcal{O}_N$. To apply the theory to the problem under consideration, the processed EMG signal (e_i) is lifted using the vector of functions ϕ , and the measured grip strength (g_i) is lifted using the vector of functions ψ . The input and output matrices with N realizations of the lifted variables (e_i, g_i) can then be written as:

$$\begin{aligned} E &= [\phi(e_1), \dots, \phi(e_N)], \\ G &= [\psi(g_1), \dots, \psi(g_N)]. \end{aligned} \quad (4)$$

The approximation of the static Koopman operator is obtained by minimizing the Frobenius norm [17]:

$$\min_{\mathcal{K}} \|G - \mathcal{K}E\|_F \rightarrow \bar{\mathcal{K}} = GE^\dagger, \quad (5)$$

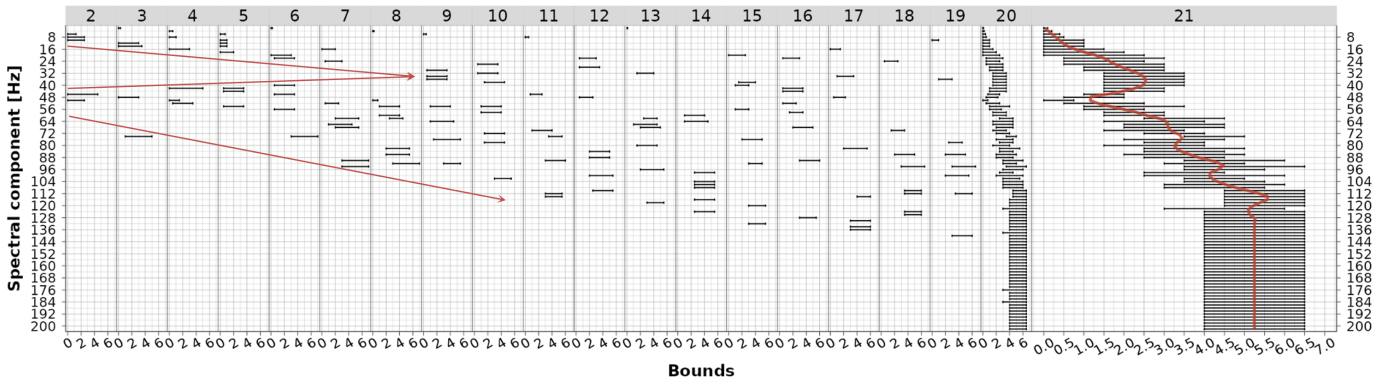


Fig. 4: Iterative multi-step sensitivity analysis (steps 2–21) and simultaneous optimization by progressively narrowing the decision vector bounds and identifying the most influential frequency components. Initial bounds were set in the 0–5 range.

where † represents the Moore-Penrose pseudoinverse. For estimations to work in real-time, it was necessary to introduce batch processing. Even though the Koopman operator was approximated using the entire calibrating dataset to obtain the final estimations, each batch was successively processed, applying the operator only to the data under the batch window. Each batch window encompasses 0.5 seconds or 496 data points. Processed EMG (Fig. 8b) was downsampled eight times before estimating grip force ($993 \rightarrow 124$ Hz) and scaled using min-max scaling to 0–1. Then, Hankel lifting using time-delay embedding was performed. Hankel data matrix E containing state \mathbf{e}_0 in the first row, and time delay embedding with d time-delayed observables in other rows with N univariate processed EMG time-series data is written as:

$$E = \begin{bmatrix} \mathbf{e}_0 \\ \mathbf{e}_{\text{id}(1)} \\ \vdots \\ \mathbf{e}_{\text{id}(d-1)} \\ \mathbf{e}_{\text{id}(d)} \end{bmatrix} = \begin{bmatrix} e_1 & e_2 & \cdots & e_{N-d} \\ e_2 & e_3 & \cdots & e_{N-d+1} \\ \vdots & \vdots & \ddots & \vdots \\ e_d & e_{d+1} & \cdots & e_{N-1} \\ e_{d+1} & e_{d+2} & \cdots & e_N \end{bmatrix}. \quad (6)$$

The same lifting was performed for both downsampled EMG (E) and grip data (G), using $d = 60$ time delays. Another nonlinear lifting, used for proper mapping between EMG and grip plateaus and perfectly fitting in KOT, is performed using gridded indicator observables. A Cartesian plane with 3 time delays is divided into subregions using a rectangular grid (Fig. 5). Each subregion is considered a separate observable. For 3 arbitrary time delays (τ_1 and τ_2 apart) and one subregion S_{ijk} , it is necessary to identify which data points fall within the selected subregion, applying an indicator function to assign a value of one to those points and zero to others. Let S_{ijk} be a subregion in $[0, 1]^3$ defined by the grid bounds:

- For $\mathbf{e}_{\text{id}(n)}[1]$: lower limit b_i , upper limit b_{i+1} .
- For $\mathbf{e}_{\text{id}(n)}[1 + \tau_1]$: lower limit b_j , upper limit b_{j+1} .
- For $\mathbf{e}_{\text{id}(n)}[1 + \tau_2]$: lower limit b_k , upper limit b_{k+1} .

The indicator function is defined as:

$$\chi_{S_{ijk}}(\mathbf{e}_{\text{id}(n)}, \tau_1, \tau_2) = \begin{cases} 1, & \text{if } b_i \leq \mathbf{e}_{\text{id}(n)}[1] \leq b_{i+1} \text{ and} \\ & b_j \leq \mathbf{e}_{\text{id}(n)}[1 + \tau_1] \leq b_{j+1} \text{ and} \\ & b_k \leq \mathbf{e}_{\text{id}(n)}[1 + \tau_2] \leq b_{k+1}, \\ 0, & \text{otherwise.} \end{cases} \quad (7)$$

Gridded indicator observable $\mathbf{e}_{I, S_{ijk}, \tau_1, \tau_2}$ can be obtained by applying (7):

$$\mathbf{e}_{I, S_{ijk}, \tau_1, \tau_2}[n] = \chi_{S_{ijk}}(\mathbf{e}_{\text{id}(n)}, \tau_1, \tau_2), \quad \text{for } n = 1, \dots, N - d. \quad (8)$$

By lifting in such a way, a lot of empty (all zero elements) and sparse (most zero elements) observables can be obtained, which may cause overfitting of the estimation model. Our approach set a constraint to keep only observables with at least 0.1% density during the algorithm testing phase to avoid overfitting. Also, the optimal grid with 22 uneven divisions (b) and a power function with exponent 1.8 for adjusting the spacing per dimension was selected during testing. Such nonlinear mapping in the form of power function was obtained by detecting plateaus in processed EMG (red line in Fig 8b) and comparing them against plateaus in measured grip force (blue line in Fig 8b). The gridding was simultaneously applied to 1st, 30th and 60th time delay ($\tau_1 = 29, \tau_2 = 59 \rightarrow \mathbf{e}_{I, S_{ijk}, 29, 59}$). The maximum possible number of gridded indicator observables using three time delays is $22^3 = 10648$, but most of them are dropped due to large sparsity. The final data matrices (E, G) for computing the static Koopman operator were constructed by vertically stacking row vectors of time-delayed observables alongside row vectors of gridded indicator observables for the processed EMG data, and rows of zeros for the grip force.

$$E = (\mathbf{e}_0, \mathbf{e}_{\text{id}(1)}, \dots, \mathbf{e}_{\text{id}(60)}, \dots, \mathbf{e}_{I, S_{ijk}, 29, 59}, \dots)^T \quad (9)$$

$$G = (\mathbf{g}_0, \mathbf{g}_{\text{id}(1)}, \dots, \mathbf{g}_{\text{id}(60)}, \dots, \mathbf{0}, \dots)^T.$$

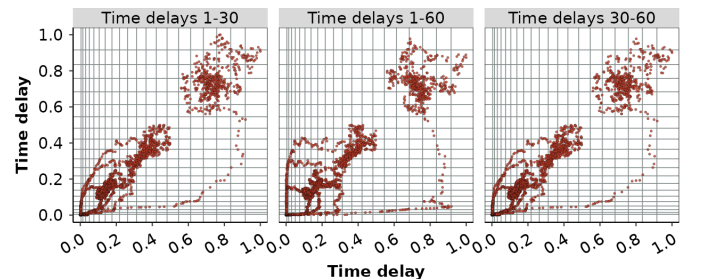


Fig. 5: Example of gridded indicator observables in three dimensions with optimal grid division.

Then, using the (5), the estimation model was learned from the entire calibrating measurement, which took less than 1.5 seconds. The obtained grip force approximation has been further thresholded to a minimum negative value of -1. The devised methodology for short-term predictions of grip force within a 0.5-second horizon is based on the previously described grip estimations and the Koopman operator for modeling dynamic systems. Again, the Koopman operator is considered appropriate due to its successful adaptation to dynamically changing environments [17], such as object grasping. Here, we aim to determine the Koopman operator for the dynamical system that governs the evolution of observables within the same space and use it for forecasting. This methodology allows for short training times on data batches, thus adapting to the latest system state. Since the Koopman operator can be infinite-dimensional, we use the dynamic mode decomposition (DMD) technique to approximate its spectral properties numerically, specifically Ritz pairs (λ_j - Ritz values, z_j - Ritz vectors):

$$\begin{aligned} \mathcal{K}Z &= Z\Lambda, \\ Z &= (z_1, \dots, z_j, \dots, z_r), \\ \Lambda &= \text{diag}(\lambda_1, \dots, \lambda_j, \dots, \lambda_r), \end{aligned} \quad (10)$$

where r represents the total number of Koopman modes after DMD. To establish a connection between the input data matrix and the spectral properties of the Koopman operator, we employed our versatile pyKMD⁷ suite. We applied the Hankel-DMD embedding [18], the Refined Rayleigh-Ritz Data-Driven Modal Decomposition (DDMD_RRR) method, and QR compression methods [19]. The DDMD_RRR method refines Ritz vectors and improves spectral accuracy by minimizing residuals in a data-driven setting, while QR compression enables efficient real-time algorithm execution. Embedding and using time-delayed observables proved effective, as the time-delayed model remained linear while capturing the non-linearities in grip force prediction. The number of time delays was kept in the 4–10 range and fine-tuned later. Before further data preparation for predictions, grip force approximation was smoothed using *Locally Weighted Scatterplot Smoothing* (LOWESS) [20], with the window size in the 1.1–1.9 batch size range and no additional iterations. For smoothing, currently processed and previous batches were used to reduce spikes, reducing prediction errors. The smoothing coefficient was fine-tuned as one of the algorithm hyperparameters. Additionally, a matrix of interactions (combinations) between \ln transformations of entries in (6) was necessary to reduce prediction error. Ten was added to the entries in (6) to keep them positive for the \ln transform. The interaction part of the input data matrix with estimated grip force $G_{e,\text{int}}$ for forecasting is:

$$G_{e,\text{int}} = \begin{bmatrix} \ln g_{e1} \ln g_{e2} & \ln g_{e2} \ln g_{e3} & \cdots & \ln g_{e(N-d)} \ln g_{e(N-d+1)} \\ \ln g_{e1} \ln g_{e3} & \ln g_{e2} \ln g_{e4} & \cdots & \ln g_{e(N-d)} \ln g_{e(N-d+2)} \\ \vdots & \vdots & \ddots & \vdots \\ \ln g_{e(d-1)} \ln g_{e(d+1)} & \ln g_{ed} \ln g_{e(d+2)} & \cdots & \ln g_{e(N-2)} \ln g_{eN} \\ \ln g_{ed} \ln g_{e(d+1)} & \ln g_{e(d+1)} \ln g_{e(d+2)} & \cdots & \ln g_{e(N-1)} \ln g_{eN} \end{bmatrix} \quad (11)$$

The input data matrix in the lifted space, obtained by stacking (11) and time delay embedding of estimated grip data, can be

written as a sequence of snapshots $\mathbf{g}_{e,\text{lift}(i)}$:

$$G_{e,\text{lift}} = \begin{pmatrix} G_{e,\text{int}} \\ G_{e,\text{td}} \end{pmatrix} = (\mathbf{g}_{e,\text{lift}(1)}, \dots, \mathbf{g}_{e,\text{lift}(N-d)}). \quad (12)$$

Before feeding the (12) to the DMD, it was further processed through a thinning step. This method is a better alternative to downsampling because it preserves data points as time delays rather than simply removing them. By thinning the data matrix before forecasting [21], the additional computational burden is reduced, and predicting higher frequency noise in the data is avoided. Using a thinning step in range 3–8, forecasts are provided with 16–41 Hz frequency, proving sufficient for the gripping dynamics. After obtaining spectral decomposition of the Koopman operator \mathcal{K} , Koopman amplitudes α_j must be computed to facilitate the reconstruction of the input data matrix or predict the next state. The problem can be formulated as a least squares minimization problem:

$$\sum_{i=1}^{N-d} \|\mathbf{g}_{e,\text{lift}(i)} - \sum_{j=1}^{\ell} z_j \alpha_j \lambda_j^{i-1}\|_2^2 \rightarrow \min, \quad (13)$$

where ℓ denotes the number of modes kept after mode reduction $r \rightarrow \ell$. Implemented solver from [22] can efficiently solve (13) using normal equations or, if the problem is ill-conditioned, a QR factorization-based solver, both of which are contained within the pyKMD framework. After obtaining predictions, as a final step, too low or too high values were thresholded to the minimum and maximum grip force from the calibrating experiment. Finally, forecasting future snapshots in horizon τ can be approximated using:

$$\mathbf{g}_{e,\text{lift}(N-d+\tau)} \approx \sum_{j=1}^{\ell} z_j \alpha_j \lambda_j^{N-d+\tau-1}, \quad \tau = 1, \dots \quad (14)$$

The reported error metric for estimating and predicting grip force is the *weighted Mean Absolute Percentage Error* (wMAPE):

$$\text{wMAPE} = \frac{\sum_{i=1}^N |\hat{g}_i - g_i|}{\sum_{i=1}^N |g_i|} \quad (15)$$

This relative metric was chosen because it effectively handles close-to-zero values by normalizing absolute errors with the sum of actual values, making it suitable for comparison across measurements with varying absolute grip magnitudes.

Final hyperparameter tuning for the prediction model was conducted using a grid search across five parameters: number of Koopman modes after reduction (ℓ), number of time delays (d), batch window modifier coefficient for smoothing, batch window modifier for prediction, and thinning step. Based on the hyperparameter tuning results shown in Fig. 6, with runs featuring extremely high errors excluded, it can be concluded that the minimum wMAPE error is achieved with four Koopman modes, 7–10 time delays, batch window modifier coefficient for smoothing in the range of 1.1–1.2, thinning step in the range of 7–8, and a batch window size modifier coefficient in the range of 1.2–1.4. To select the final hyperparameters for the prediction algorithm, the median wMAPE value across all measurements was also computed to enhance metric robustness. The hyperparameters resulting in

⁷<https://apps.aimdyn.com/>

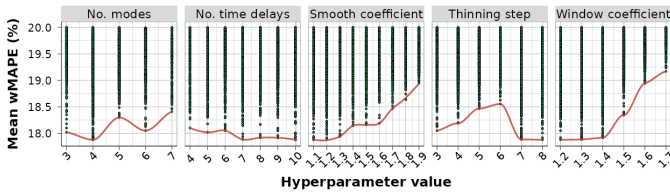


Fig. 6: Hyperparameter tuning runs for optimizing prediction algorithm. wMAPE is an average of all predictions across all 52 experiments. A smooth red line connects the minimum run values for hyperparameter levels.

the minimal sum of mean and median wMAPE are presented in Table V. The final reported error metric using these optimal hyperparameters can be found in Table VI.

III. RESULTS & EXPERIMENTAL VALIDATION

The analysis of the most sensitive frequencies from the multi-step SA (Fig. 4) shows the need to first act on reducing the lower frequency spectral components (≤ 14 Hz) and those in the 46–50 Hz range to improve the peak cross-correlations between the processed EMG signal and the measured grip strength. Once the bounds of these initial sensitive spectral components are narrowed to near-optimal values, the range of sensitive frequencies expands, filling the gap between 14 and 46 Hz and extending towards higher-frequency components (arrows in Fig. 4). Typically, parameter optimization would be performed within the narrowed decision vector bounds. However, it is unnecessary in this case due to the descriptive statistics of the resulting average peak cross-correlation computed from all LH samples after the final SA step. Descriptive statistics for different positions are as follows:

- P1: mean 0.956, SD 0.000413, min. 0.954, max. 0.958,
- P2: mean 0.960, SD 0.000535, min. 0.958, max. 0.962.

Because the standard deviation of the average peak cross-correlations indicates extremely low variability, the mean values between each decision variable’s upper and lower bounds will be used as the optimal mask values, as shown in Fig. 7. Table II presents summary statistics of peak cross-correlations for all measurements at both sensing positions, revealing very strong correlations between optimal processed EMG signals and measured grip force. The analysis reveals that the EMG signals lag behind the grip force measurements, with lags varying between 0 and 156 ms.

Sections of the optimal spectral mask align with findings from the literature [15], where lower-frequency components associated with wire movements are either attenuated or removed. The attenuation is nearly linear, with DC component and 2 Hz fully filtered out, 10 Hz reduced by 50%, and 18 Hz left unaffected. Frequencies between 20 and 48 Hz require amplification following an inverted U-shaped curve, starting and ending at 25%, with a peak amplification of 150% between 32 and 42 Hz. The inverted U is followed by a sharp dip at the 50 Hz component, indicating that electrical ground noise impacts the recorded signal. The 50 Hz spectral component proves particularly challenging to process, as neither retaining it at nominal amplitudes (typically done with a bandpass filter)

	Min.	1st Qu.	Median	Mean	3rd Qu.	Max.
Position 1						
Peak cross-correlation	0.891	0.947	0.964	0.958	0.971	0.987
Optimal time lag [ms]	0.0	0.0	43.8	54.0	96.4	156.1
Position 2						
Peak cross-correlation	0.924	0.952	0.967	0.962	0.972	0.988
Optimal time lag [ms]	0.0	0.0	16.1	25.0	42.8	78.5

TABLE II: Cross-correlation summary statistics: Optimal processed EMG signals – grip force for all measurements on two sensing positions.

nor completely removing it (using a notch filter) is sufficient. Our optimizations show that maintaining 50 Hz at 37.5% of its amplitude preserves enough of the signal’s power for grip force modeling. This finding supports the conclusions of [15], which state that a significant portion of the EMG signal’s power spectrum is concentrated at 50 Hz and should not be entirely filtered out. The next section of the mask targets amplifying the mid-frequency spectra, where most of the signal’s power is concentrated. As the amplitudes of the spectral components decrease, the mask progressively amplifies them, increasing approximately linearly from 50% at 52 Hz to 450% at 110 Hz. This amplification trend plateaus at 425–450% around 110 Hz and extends up to 202 Hz. A possible explanation for the need to amplify mid-frequency spectral components may lie in three physiological phenomena related to the spatial low-pass filtering of recorded EMG signals: MU structure, volume conduction, and electrode positioning [1]. First, the MU structure introduces spatial smoothing at the signal source due to the scattered arrangement of muscle fibers within a MU. Volume conduction refers to the signal’s attenuation and distortion as it propagates through biological tissues from the source to the skin surface, where it is measured. Finally, electrode positioning contributes to low-pass filtering, as the electrodes capture an averaged signal over the area they cover, further reducing higher-frequency content. We conducted a stepwise ablation study on the spectral mask plateau (110–202 Hz) to validate our conclusions. We systematically excluded frequency bands in 4 Hz increments, starting from 110–202 Hz and progressing to 198–202 Hz. Each step resulted in a lower-than-optimal mean peak cross-correlation between processed EMG and measured grip force. Our SA revealed the minimal influence of higher-frequency components (204–498 Hz). We performed an additional ablation study by varying the mask from 0 to 5 in this range. As no significant changes in mean peak cross-correlation were observed, we set the mask to 0 for the 204–498 Hz range, effectively shielding the system from potential noise in this band. This approach to processing sEMG signals is innovative, and some of the resulting observations warrant further investigation for a clearer understanding. By applying the signal processing methods outlined in section II-B, the processed EMG signals, shown in red in Fig. 8b, demonstrate a clear high cross-correlation with the measured grip force.

The employed RBD experimental design allows for investigating the effects of subject and sensing location (position) on the wMAPE estimation metric. Using the procedure described

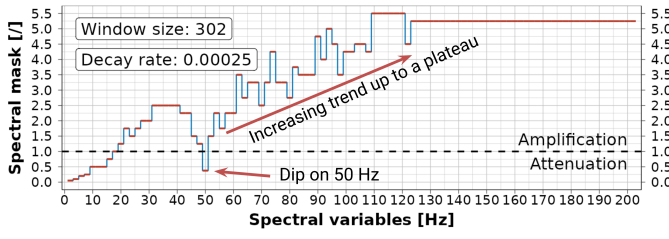


Fig. 7: Optimal spectral mask for filtering measured EMG signal on positions 1 and 2.

Subject														Position	
ac	dp	ds	js	lb	lk	lm	ln	md	mm	nk	pb	ss	M	E	
Position 1															
R1	4.4	6.4	10.0	4.5	7.7	6.6	4.5	8.4	4.3	5.1	2.7	6.1	3.8		
R2	2.3	4.7	5.4	3.9	8.0	6.9	7.6	3.7	5.2	6.8	6.4	7.9	4.3	5.7	0.2
Position 2															
R1	4.0	4.1	4.7	3.9	3.3	5.8	3.6	4.4	7.2	8.5	3.3	6.7	4.4		
R2	3.8	4.3	4.4	5.1	4.9	6.2	4.4	4.6	9.2	9.9	3.2	10.1	3.3	5.3	-0.2
Subject mean and effect															
M	3.6	4.9	6.1	4.4	6.0	6.4	5.1	5.3	6.5	7.6	3.9	7.7	4.0		
E	-1.8	-0.6	0.6	-1.1	0.5	0.9	-0.4	-0.2	1.0	2.1	-1.6	2.2	-1.5		

Overall estimation mean wMAPE: 5.48%

TABLE III: wMAPE for estimating grip force from EMG per subject and position. (R: Replication; M: Mean; E: Effect)

in section II-C, wMAPE estimation error was calculated for each of the 52 experiment runs and is presented in Table III. The overall mean estimation wMAPE is approximately 5.5%, demonstrating the effectiveness of this approach in accurately approximating grip force using a single sensing position. In addition to single-measurement error metrics, we computed means and effects across blocks containing all measurements for each position and subject. The effects were computed as the difference between the block mean and the overall mean wMAPE. Although the means and effects varied considerably across subjects, the mean for sensing position 1 was only 0.2% worse than the overall mean, while the mean for position 2 was 0.2% better. An analysis of variance (ANOVA) was conducted on the blocked RBD with estimation wMAPE to assess the significance of the position effect using a 5% significance level. The results, presented in Table IV, show that, while the effect of the subject on wMAPE was significant (p -value = 0.015), the effect of position (when the subject effect is removed) was not (p -value = 0.422). It can be concluded that the placement of EMG electrodes along the flexor carpi ulnaris muscle, whether in position 1 or 2, does not significantly influence the estimation error. Three representative examples of estimated grip force, with errors corresponding approximately to the first, second, and third quartiles, are highlighted in yellow in Fig. 8b. The complete set of graphs is available in the first author's GitHub repository⁸.

Following a similar approach to the estimations, the methodology from section II-C was applied to short-term forecasts of grip force in 0.5-second batches within a 0.5-second horizon.

⁸<https://github.com/tbazina/grip-emg-optimize>

Estimation								Prediction							
Df	Sum Sq	Mean Sq	F value	Pr(>F)	Df	Sum Sq	Mean Sq	F value	Pr(>F)	Df	Sum Sq	Mean Sq	F value	Pr(>F)	Df
Position	1	1.91	1.91	0.66	0.422	1	0.35	0.35	0.03	0.853					
Subject	12	87.51	7.29	2.52	0.015	12	232.00	19.33	1.94	0.060					
Residuals	38	110.15	2.90			38	378.55	9.96							

TABLE IV: RBD results - non-significant effect of measuring position on wMAPE.

Batch window size	Batch modifier	Thin-	No.	No.
modifier coefficient	coefficient for smoothing	ning step	time delays	Koopman modes
1.3	1.1	7	8	4

TABLE V: Optimal hyperparameters for prediction model obtained after tuning results for prediction algorithm.

Subject														Position	
ac	dp	ds	js	lb	lk	lm	ln	md	mm	nk	pb	ss	M	E	
Position 1															
R1	24.7	15.0	25.0	18.7	21.4	21.1	13.1	22.7	12.5	15.4	19.4	18.8	13.4		
R2	23.6	15.4	17.9	17.6	15.0	18.9	17.5	15.1	22.3	14.7	18.6	19.6	10.6	18.0	0.1
Position 2															
R1	14.8	17.2	16.7	17.7	16.1	20.4	12.9	18.5	15.8	17.2	19.1	20.2	15.2		
R2	16.8	16.1	17.6	22.3	14.2	22.9	12.3	17.2	20.9	25.2	19.0	20.5	16.7	17.8	-0.1
Subject mean and effect															
M	20.0	15.9	19.3	19.1	16.7	20.9	13.9	18.4	17.9	18.2	19.0	19.8	14.0		
E	2.1	-2.0	1.4	1.2	-1.3	2.9	-4.0	0.4	-0.0	0.2	1.1	1.8	-4.0		

Overall prediction mean wMAPE: 17.92%

TABLE VI: wMAPE for predicting grip force from EMG per subject and position. (R: Repetition; M: Mean; E: Effect)

wMAPE errors were computed for all measurements and reported as RBD results in Table VI. We used the optimal hyperparameters from Table V and achieved approximately 17.9% overall forecast wMAPE. While the effect of the subject varied, the effect of position on wMAPE remained within the ± 0.1 range. The ANOVA analysis in Table IV again confirmed the non-significant effect of position on forecast error (p -value = 0.853), and this time, the effect of the subject was also non-significant (p -value = 0.06). These conclusions further demonstrate the method's robustness to electrode placement along the flexor carpi ulnaris muscle. Examples of forecasts with error metric values approximately corresponding to the first, second, and third quartiles are shown as red dots in Fig. 8c, with the smoothed grip force estimation, which serves as the input signal for forecasting, displayed in yellow. Fig. 8 contrasts all described sEMG and grip signals, from raw and processed EMG to estimated and measured grip force, topping in smoothed estimates and short-term batch predictions.

IV. CONCLUSION

This research focuses on developing real-time procedures for sensing hand muscle activity and estimating the exerted force by a subject, with potential applications in controlling rehabilitation devices and tracking patient recovery between rehabilitation sessions. The methodology involves sensing muscle activity (physiological signals) using non-invasive surface electromyography (sEMG) sensors. The signals are

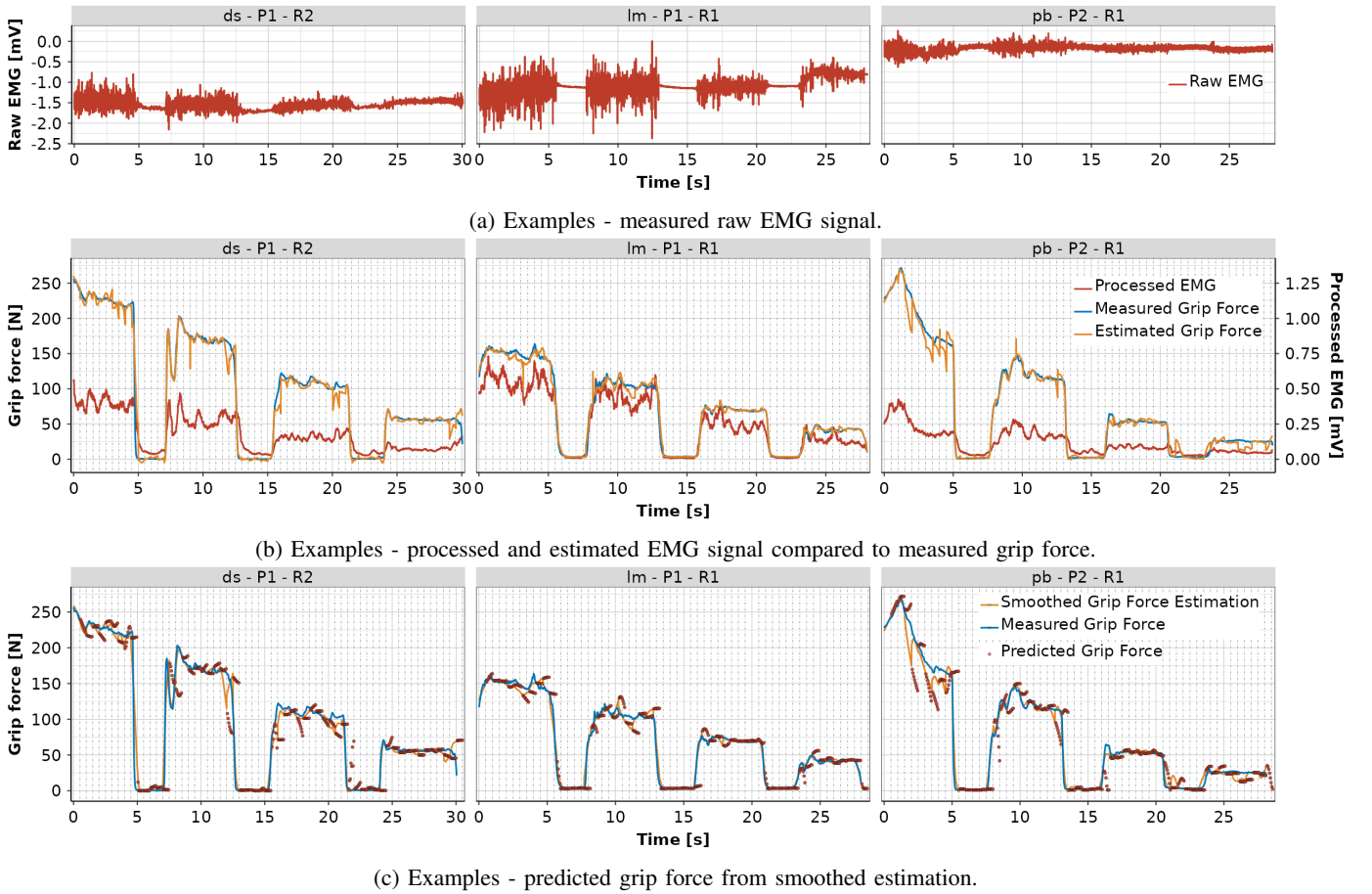


Fig. 8: Examples of all signals relevant for grip force modeling - raw and processed EMG signals, estimates, smoothed estimates, forecasts, and measured grip force.

cross-correlated with synchronously collected hand grip force, determined using a force-calibrated hand dynamometer as part of a properly designed experiment. We devise the composition of the sEMG signal processing steps to achieve a strong peak cross-correlation ($\sim 96\%$) between meaningful muscle activity and grip force. We optimized decision variables to maximize cross-correlation: spectral mask, smoothing window size, and decay rate. Finally, we employed a data-driven approach using only the processed EMG signal acquired from a single sensing location. The static Koopman operator was utilized for accurate force estimation, while the Koopman operator for dynamic systems was used for short-term grip force prediction. The algorithm follows these steps within the framework: processing raw EMG data, transforming and lifting the data for estimation, applying the estimation model, smoothing the estimates and lifting them for prediction, training the prediction model online, and generating forecasts.

The Koopman-based methodology proved efficient, with an average weighted mean absolute percentage error of approximately 5.5% for estimations and 17.9% for predictions. Additionally, the method proved robust to varying sensing locations, as its effectiveness was evaluated at two different measurement points. It requires less than 30 seconds to perform a one-time, patient-specific calibrating experiment using both sEMG sensors and a hand dynamometer, followed by 1.5 seconds

for estimation model training. The experimental assessment demonstrated rapid execution, requiring only 30 ms to generate 0.5-second predictions once the last 0.5-second data batch is received. Consequently, the developed framework is ready for real-time implementation.

Future work will integrate the developed Robot Operating System (ROS) modules for interacting with sensors, data acquisition, and signal processing with a real-time Koopman-driven hand grip force estimation and prediction module, based on the methods presented in Section II-C. Additionally, the advancements in simplifying hand kinematics presented in [23] will be incorporated to develop a comprehensive system, including a human agent model with various grasp modalities. This holistic approach aims to accelerate the development of sophisticated robotic rehabilitation devices, enhancing their effectiveness and adaptability to individual patient needs.

ACKNOWLEDGMENT

The authors thank their students for conducting initial experiments and providing the experimental data. This material is based upon work supported by the Air Force Office of Scientific Research under award number FA9550-22-1-0531 and by the University of Rijeka under Grant uniri-iskusni-tehnic-23-4.

REFERENCES

- [1] D. F. Stegeman, J. H. Blok, H. J. Hermens, and K. Roeleveld, "Surface emg models: Properties and applications," *Journal of Electromyography and Kinesiology*, vol. 10, no. 5, pp. 313–326, Oct. 2000, ISSN: 1050-6411. DOI: 10.1016/s1050-6411(00)00023-7.
- [2] R. Ma, L. Zhang, G. Li, D. Jiang, S. Xu, and D. Chen, "Grasping force prediction based on semg signals," *Alexandria Engineering Journal*, vol. 59, no. 3, pp. 1135–1147, Jun. 2020, ISSN: 1110-0168. DOI: 10.1016/j.aej.2020.01.007.
- [3] S. M. Khan, A. A. Khan, and O. Farooq, "An early force prediction control scheme using multimodal sensing of electromyography and digit force signals," *Heliyon*, vol. 10, no. 8, e28716, Apr. 2024, ISSN: 2405-8440. DOI: 10.1016/j.heliyon.2024.e28716.
- [4] R. Barański and A. Kozupa, "Hand grip-EMG muscle response," *Acta Physica Polonica A*, vol. 125, no. 4A, A-7–A-10, Apr. 2014. DOI: 10.12693/aphyspola.125.a-7.
- [5] A. G. Siavashani, A. Yousefi-Koma, and A. Vedadi, "Estimation and early prediction of grip force based on sEMG signals and deep recurrent neural networks," *Journal of the Brazilian Society of Mechanical Sciences and Engineering*, vol. 45, no. 5, Apr. 2023. DOI: 10.1007/s40430-023-04070-8.
- [6] N. Zhang, K. Li, G. Li, R. Nataraj, and N. Wei, "Multiplex recurrence network analysis of inter-muscular coordination during sustained grip and pinch contractions at different force levels," *IEEE Transactions on Neural Systems and Rehabilitation Engineering*, vol. 29, pp. 2055–2066, 2021. DOI: 10.1109/tnsre.2021.3117286.
- [7] I. J. R. Martinez, A. Mannini, F. Clemente, A. M. Sabatini, and C. Cipriani, "Grasp force estimation from the transient EMG using high-density surface recordings," *Journal of Neural Engineering*, vol. 17, no. 1, p. 016052, Feb. 2020. DOI: 10.1088/1741-2552/ab673f.
- [8] I. J. R. Martinez, A. Mannini, F. Clemente, and C. Cipriani, "Online grasp force estimation from the transient EMG," *IEEE Transactions on Neural Systems and Rehabilitation Engineering*, vol. 28, no. 10, pp. 2333–2341, Oct. 2020. DOI: 10.1109/tnsre.2020.3022587.
- [9] C. Wu, Q. Cao, F. Fei, *et al.*, "Optimal strategy of semg feature and measurement position for grasp force estimation," *PLOS ONE*, vol. 16, no. 3, L. Wen, Ed., e0247883, Mar. 2021, ISSN: 1932-6203. DOI: 10.1371/journal.pone.0247883.
- [10] I. Mezić, "Spectral properties of dynamical systems, model reduction and decompositions," *Nonlinear Dynamics*, vol. 41, pp. 309–325, 2005.
- [11] M. Cutkosky, "On grasp choice, grasp models, and the design of hands for manufacturing tasks," *IEEE Trans. Robot. Automat.*, vol. 5, no. 3, pp. 269–279, Jun. 1989. DOI: 10.1109/70.34763.
- [12] T. Feix, J. Romero, H.-B. Schmiedmayer, A. M. Dollar, and D. Kragic, "The grasp taxonomy of human grasp types," *IEEE Transactions on Human-Machine Systems*, vol. 46, no. 1, pp. 66–77, Feb. 2016, ISSN: 2168-2305. DOI: 10.1109/thms.2015.2470657.
- [13] N. A. Heckert, J. J. Filliben, C. M. Croarkin, *et al.*, *Nist/sematech e-handbook of statistical methods (nist handbook 151)*, 2012. DOI: 10.18434/M32189.
- [14] S. Tarantola, D. Gatelli, and T. Mara, "Random balance designs for the estimation of first order global sensitivity indices," *Reliability Engineering & System Safety*, vol. 91, no. 6, pp. 717–727, Jun. 2006, ISSN: 0951-8320. DOI: 10.1016/j.res.2005.06.003.
- [15] P. Konrad, *The ABC of EMG - A practical introduction to kinesiological electromyography*. Noraxon U.S.A. Inc., 2006, vol. 1, pp. 30–5, ISBN: 0-9771622-1-4.
- [16] P. J. Schmid, "Dynamic mode decomposition and its variants," *Annual Review of Fluid Mechanics*, vol. 54, no. 1, pp. 225–254, Jan. 2022. DOI: 10.1146/annurev-fluid-030121-015835.
- [17] I. Mezić, "Koopman operator, geometry, and learning of dynamical systems," *Not. Am. Math. Soc.*, vol. 68, no. 7, pp. 1087–1105, 2021.
- [18] H. Arbabi and I. Mezić, "Ergodic theory, dynamic mode decomposition, and computation of spectral properties of the koopman operator," *SIAM Journal on Applied Dynamical Systems*, vol. 16, no. 4, pp. 2096–2126, Jan. 2017, ISSN: 1536-0040. DOI: 10.1137/17m1125236.
- [19] Z. Drmač, I. Mezić, and R. Mohr, "Data driven modal decompositions: Analysis and enhancements," *SIAM Journal on Scientific Computing*, vol. 40, no. 4, A2253–A2285, Jan. 2018. DOI: 10.1137/17m1144155.
- [20] W. S. Cleveland, "Robust locally weighted regression and smoothing scatterplots," *Journal of the American Statistical Association*, vol. 74, no. 368, pp. 829–836, Dec. 1979, ISSN: 1537-274X. DOI: 10.1080/01621459.1979.10481038.
- [21] P. Frame and A. Towne, "Space-time POD and the hankel matrix," *PLOS ONE*, vol. 18, no. 8, M. K. Riahi, Ed., e0289637, Aug. 2023, ISSN: 1932-6203. DOI: 10.1371/journal.pone.0289637.
- [22] Z. Drmač, I. Mezić, and R. Mohr, "On least squares problems with certain vandermonde–khatri–rao structure with applications to DMD," *SIAM Journal on Scientific Computing*, vol. 42, no. 5, A3250–A3284, Jan. 2020. DOI: 10.1137/19m1288474.
- [23] T. Bazina, G. Mauša, S. Zelenika, and E. Kamenar, "Reducing hand kinematics by introducing grasp-oriented intra-finger dependencies," *Robotics*, vol. 13, no. 6, p. 82, May 2024, ISSN: 2218-6581. DOI: 10.3390/robotics13060082.